# Analyst

## Accepted Manuscript

This article can be cited before page numbers have been issued, to do this please use: Y. Zang, Y. Ju, J. Jiang, Q. Xu, M. Chu and H. Xue, *Analyst*, 2019, DOI: 10.1039/C9AN00636B.

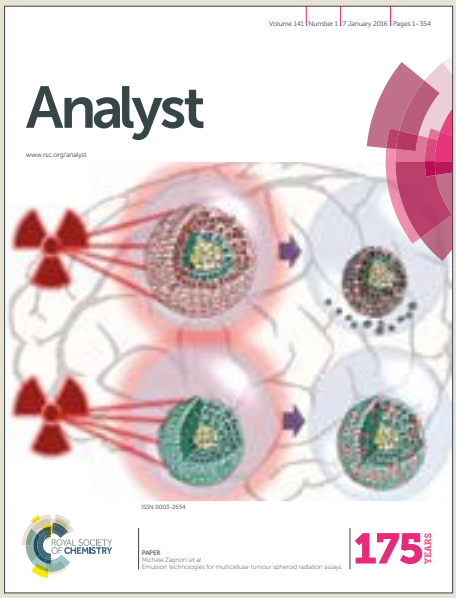




ROYAL SOCIETY OF CHEMISTRY

rsc.li/analyst

Journal Name

ROYAL SOCIETY OF CHEMISTRY View Article Online
DOI: 10.1039/C9AN00636B

ARTICLE

# $Cu^{2+}$-modulated in situ growth of quantum dots for split-type photoelectrochemical immunoassay of prostate specific antigen

Received 00th January 20xx,
Accepted 00th January 20xx

DOI: 10.1039/x0xx00000x

www.rsc.org/

Yang Zang,[a]* Yun Ju,[a] Jingjing Jiang,[a]* Qin Xu,[a] Ming Chu[b] and Huaiguo Xue[a]

A split-type photoelectrochemical immunosensor was designed for ultrasensitive monitoring of prostate specific antigen (PSA) based on $Cu^{2+}$-mediated catalytic reaction for inhibiting the in situ generation of CdS quantum dots (QDs) coupled with the enhancement effect of CdS/$MoS_2$ heterojunction, which was constructed by the stepwise modification of $MoS_2$ QDs and CdS QDs on ITO electrode surface. In the presence of PSA, CuO NPs-labeled anti-PSA antibody was immobilized onto anti-PSA antibody modified 96-well plate via sandwich immunoreaction, and dissolved by hydrochloric acid to obtain a large number of $Cu^{2+}$. As $Cu^{2+}$-triggered catalytic oxidization of glutathione occurred, in situ growth of CdS QDs as signal indicator was significantly suppressed, resulting in the reduction of photocurrent response. Under optimal conditions, the biosensor exhibited the desirable linearity in the range from 0.5 pg $mL^{-1}$ to 10 ng $mL^{-1}$, low detection limit of 0.29 pg $mL^{-1}$, satisfactory selectivity, good stability, and was applied to PSA detection in human serum, holding great potential for early diagnostics of some cancer diseases.

## Introduction

As the development of life quality and health awareness, people have paid more attention to their medical security and life safety, which arouses interest in exploiting the ingenious sensing devices for the detection of trace disease markers at very early stage. Among them, prostate specific antigen (PSA) is a glycoprotein generated by prostate tissues, and usually remains below 4 ng $mL^{-1}$ in normal male serum.[1–3] The rapid ascension of serum PSA level is identified as the important indicator for prostate cancer, which becomes one of the biggest concerns due to its high incidence and heartbreaking mortality.[4–6] Thus, the early diagnosis of prostate cancer is crucial to save the threaten lives, and searching for a facile and highly sensitive PSA detection method is great significance for the continuous improvement of medical service in demand.

Photoelectrochemistry (PEC)-based immunoassay, a booming sensing technique, has particular superiority in background signal and detection sensitivity in comparison with traditional electrochemical methods owing to the different energy forms of excitation light and photocurrent signal.[7–11] Meanwhile, it is found that the higher sensitivity of photoelectrochemical immunosensor can be achieved by means of simplified modification procedures and suitable signal amplification. On the one hand, since the assembly of biomolecules onto electrode surface not only causes the decrease of photocurrent response because of stereo-hindrance effect but also weakens their own bioactivity stemmed from light irradiation and photoactive materials, the selection of split-type detection mode will efficiently avoid the mutual disturbance between biomolecules and photoelectrochemical measurement, in which biological recognition region is separated from detection system.[12,13] For example, Yang et al. reported a split-type photoelectrochemical immunosensor for ultrasensitive detection of HIV-p24 antigen with a low detection limit of 0.63 pg $mL^{-1}$ because the separation of light excitation and liposomes-based signal amplification eliminated the biomolecules damage.[14] On the other hand, nanoparticle-based signal amplification is usually adopted for trace and quantitative analysis without the denaturation and leakage of enzyme. Based on the merits of considerably stable and easily conjugation with antibodies, CuO nanoparticles (NPs) as $Cu^{2+}$ source are usually used in immunoassays, which can oxidize thiol reagents into disulfide compounds in the presence of $O_2$, achieving the amplified detection signal.[15–17] Inspired by this catalytic ability, in situ growth of CdS quantum dots (QDs) can be regulated by $Cu^{2+}$-initiated catalytic oxidization of glutathione (GSH) as stabilizer.[18] Especially, compared with pre-synthesized CdS QDs, the utilization of QDs in situ formed can reduce the modification processes, decrease the background signal, avoid the particle aggregation and photocorrosion after long-term storage.[19–21]

Moreover, to further enhance the detection sensitivity, great

[a] School of Chemistry and Chemical Engineering, Yangzhou University, Yangzhou, 225002, Jiangsu, China. E-mail: zangyang@yzu.edu.cn, jjj@yzu.edu.cn;
[b] The First Affiliated Hospital with Nanjing Medical University, Nanjing, Jiangsu, 210029, P. R. China

Electronic Supplementary Information (ESI) available: Experimental apparatus utilized in this work, preparation of $MoS_2$ QDs, preparation of CuO-$Ab_2$ conjugates, TEM images of CuO NPs and CuO-$Ab_2$ conjugates, EIS of bare ITO, $MoS_2$/ITO and CdS/$MoS_2$/ITO electrodes, Optimization of $Na_2S$ concentration and incubation time of PSA with $Ab_1$, comparison of the analytical performance of our work with other immunosensing methods and detection results and recoveries of PSA in human serum samples. See DOI: 10.1039/x0xx00000x.

View Article Online
DOI: 10.1039/C9AN00636B



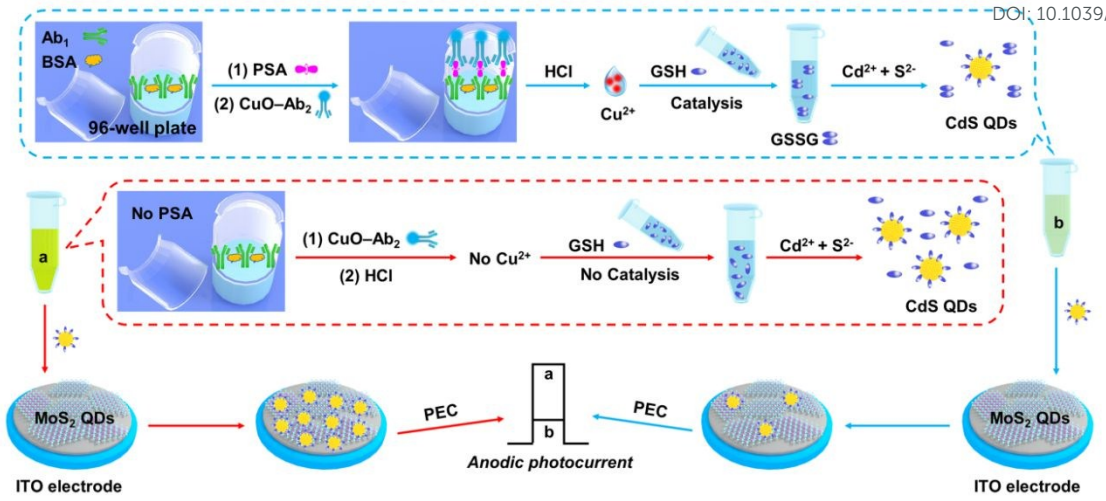


**Scheme 1** Fabrication and sensing strategy of photoelectrochemical immunosensor for ultrasensitive monitoring of PSA.

efforts have been made to facilitate the charge carrier separation
of QDs by establishing efficient heterostructure with various semiconductors. Molybdenum disulfide ($MoS_2$) nanomaterials, consisting of S-Mo-S triple atom layers bounded by van der Waals forces,[22,23] have been recognized as emerging candidates to improve the photocatalytic activity of CdS because the electron migration from CdS to $MoS_2$ was dramatically accelerated.[24–26] For example, CdS NPs/$MoS_2$ nanosheets-based hybrid possessed the improved photocatalytic ability toward $H_2$ evolution, indicating an effective inhibition for the recombination of photoexited electron-hole pairs.[27] In particularly, recent studies show that more exposed catalytic edge sites and better uniform size distribution are available when $MoS_2$ nanosheets convert to the structure of quantum dots [28–30]. However, $MoS_2$ QDs-based photoelectrochemical immunoassay study has been less reported due to their unfavourable biomolecule modification. So, the combination of $MoS_2$ QDs and in situ formed CdS QDs is benefited to construct a versatile photoelectrochemical detection platform.

In this work, a novel split-type photoelectrochemical immunosensor was facilely designed for ultrasensitive detection of PSA based on $Cu^{2+}$-dependent catalytic reaction for regulating the formed CdS QDs in situ and the signal enhancement of CdS/$MoS_2$ heterostructure, where CuO NPs-labeled anti-PSA antibody (CuO-$Ab_2$) served as amplifier and GSH as stabilizing agent of CdS QDs. Upon addition of target PSA onto anti-PSA antibody ($Ab_1$) modified 96-well plate, CuO-$Ab_2$ can be immobilized via sandwich-type immunoreaction (Scheme 1). After acid dissolution of CuO-$Ab_2$, an abundance of $Cu^{2+}$ was obtained, and then catalyzed the oxidization of GSH to reduce the amount of in situ formed CdS QDs, which was the efficient indicator further coated onto $MoS_2$ QDs modified indium tin oxide (ITO) electrode, resulting in a reduced photocurrent response. In addition, the high precision and low detection limit of proposed immunosensor are assured by virtue of split-type detection mode and nanoparticle-mediated signal amplification.

## Experimental section

### Materials and reagents

ITO electrodes were purchased from Zhuhai Kaivo Electronic Components Co., Ltd. (China). Bovine serum albumin (BSA) and ascorbic acid (AA) were bought from Sangon Biotech. Co., Ltd. (Shanghai, China). CuO NPs, GSH, $MoS_2$ power and $Cd(Ac)_2$ were obtained from Sigma-Aldrich. The monoclonal $Ab_1$, $Ab_2$, PSA, carcinoembryonic antigen (CEA) and alpha-fetoprotein (AFP) were obtained from Shanghai Linc-Bio Science Co., Ltd. The high-binding polystyrene 96-well plates were purchased from Greiner Bio-One (Frickenhausen, Germany). All the reagents were of analytical grade and used without further purification. All aqueous solutions were prepared by deionized water from a Millipore water purification system (≥18 MΩ·cm, Milli-Q, Millipore).

### Construction and test of photoelectrochemical immunosensor

Prior to the construction of photoelectrochemical immunosensor, ITO electrode was cleaned in boiling 2-propanol solution containing 1.0 M NaOH for 15 min, followed by ultrasonic treatments with 10% $H_2O_2$, acetone and deionized water, respectively. After blow-dried with nitrogen, 10 μL of $MoS_2$ QDs was applied to ITO electrode, and dried at room temperature. Then, 10 μL of in situ formed CdS QDs was coated to obtain CdS/$MoS_2$/ITO electrode via a non-covalent interaction, which was employed for photoelectrochemical measurements in 0.1 M PBS of pH 7.4 containing 0.1 M AA with a bias voltage of 0 V (versus Ag/AgCl).

Among them, the in situ generated CdS QDs were modulated as follows: First, the high-binding polystyrene 96-well plate was modified with 50 μL of 10 μg $mL^{-1}$ $Ab_1$ as capture probe for overnight at 4 °C, and was then rinsed three times by washing buffer (10 mM PBS of pH 7.4 containing 0.05% Tween 20) to remove the excess $Ab_1$. After the addition of 200 μL of 10 mM PBS of pH 7.4 containing 1% (w/v) BSA for 2 h to block the nonspecific binding sites, different concentrations

View Article Online
DOI: 10.1039/C9AN00636B



of PSA in 50 μL of 10 mM PBS of pH 7.4 were added and incubated for 40 min at 37.1 °C. Subsequently, CuO-$Ab_2$ conjugates were incubated in 96-well plate for 60 min, and 30 μL of 1 mM HCl was dropped into each plate for 5 min to release a large number of $Cu^{2+}$. Following that, 4 μL of 10 mM GSH and 5 μL of collected $Cu^{2+}$ were incubated in 10 mM citrate buffer of pH 3.5 containing 10 mM KBr for 1 min under dark conditions. Then, 10 μL of 0.25 mM $Na_2S$ and 10 μL of 10 mM $Cd(Ac)_2$ were sequentially added into the above mixture, and reacted for 5 min under vigorously vibration. It is worth noting that the above plate was rinsed by washing buffer after each assembly step. Moreover, the control experiments for other proteins were tested in the same way.

## Results and discussion

### Characterizations of $MoS_2$ QDs, CuO-$Ab_2$ and in situ formed CdS QDs

The characterizations of $MoS_2$ QDs were investigated in Fig. 1. Compared with the SEM image of bulk $MoS_2$ (Fig. 1A), the TEM image of $MoS_2$ QDs clearly revealed a highly dispersed and round-shaped morphology with an average size of 3.2 nm (Fig. 1B). Moreover, the thickness of $MoS_2$ QDs affected the Raman peak positions and intensities of in-plane $E_{2g}^1$ and out-of-plane $A_{1g}$ vibrational modes of Mo-S bond. As indicated in Fig. 1C, two characteristic peaks at around 378.4 $cm^{-1}$ and 404.0 $cm^{-1}$ were observed for bulk $MoS_2$ (curve a), as well as around 380.0 $cm^{-1}$ and 402.4 $cm^{-1}$ for exfoliated $MoS_2$ QDs (curve b), which was well-matched with the corresponding $E_{2g}^1$ and $A_{1g}$ phonon modes, respectively.[31] The lower intensity and frequency difference between $A_{1g}$ and $E_{2g}^1$ modes implied that $MoS_2$ QDs consisted of few-layered structure.[32]

The optical properties of $MoS_2$ QDs were investigated by fluorescence spectroscopy (Fig. 1D). The synthesized $MoS_2$ QDs exhibited a light yellow and transparent solution (inset in Fig. 1D), and a strong peak at 420 nm presented a direct band-edge recombination.[33] In addition, XPS measurements were further performed to investigate the chemical compositions and atomic valence states of $MoS_2$ QDs. From the high resolution XPS of Mo 3d, two main peaks at 228.1 eV and 230.9 eV corresponded to Cd $3d_{5/2}$ and Cd $3d_{3/2}$ levels, and a new small peak located at 226.0 eV was attributed to the S 2s (Fig. 1E), indicating that Mo atoms predominantly existed as $Mo^{4+}$ in our sample.[34,35] Similarly, S $2p_{3/2}$ and S $2p_{1/2}$ at 162.1 eV and 163.5 eV were observed in Fig. 1F due to the existence of $S^{2-}$ state.[36]

Fig. 2A showed that in situ formed CdS QDs were quasi-spherical granules with a mean diameter of 3.1 nm, which agreed well with the average hydrodynamic diameter of 3.7 nm recorded by dynamic light scattering (DLS) spectrum (Fig. 2B). Besides, to verify the assembly of CuO NPs with $Ab_2$, TEM images of CuO NPs and CuO-$Ab_2$ conjugates were acquired for comparison. From the Fig. S1A we could see that the average size of CuO NPs tended to be 38 nm, while that of CuO-$Ab_2$ conjugates measured up to be ~60 nm without aggregation (Fig. S1B), supporting that $Ab_2$ was modified as expected.[37]

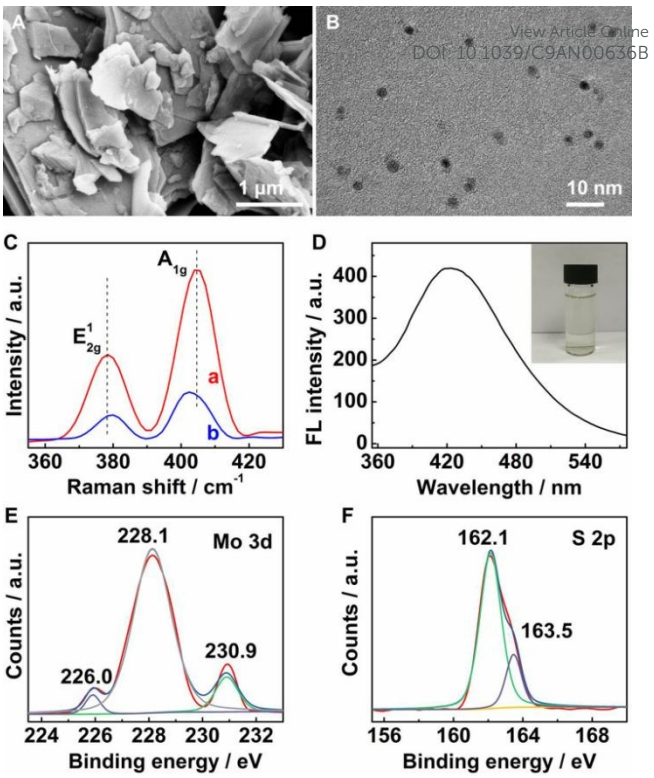


**Fig. 1** (A) SEM image of bulk $MoS_2$. (B) TEM image of $MoS_2$ QDs. (C) Raman spectra of bulk $MoS_2$ (a) and $MoS_2$ QDs (b). (D) Fluorescence, (E) Mo 3d, and (F) S 2p states-based high-resolution XPS spectra of $MoS_2$ QDs. Inset of panel D is the image of $MoS_2$ QDs solution.

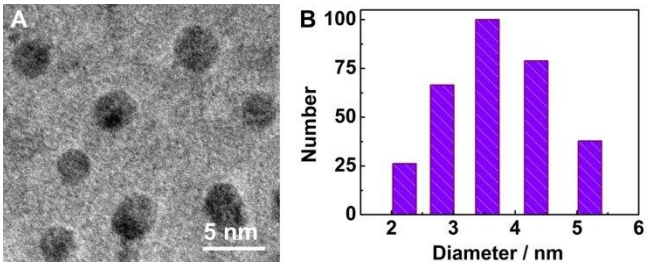


**Fig.2** (A) TEM image and (B) DLS spectrum of CdS QDs in situ formed.

### Feasibility of photoelectrochemical immunosensor

UV–vis absorption spectra were carried out to study $Cu^{2+}$-triggered catalytic process for GSH oxidization. As displayed in Fig. 3A, there was an absorbance peak at 261 nm for GSH (curve a), and a distinct shoulder at 300 nm appeared when $Cu^{2+}$ was added to stimulate the formation of GS-$Cu^{+}$-SG complex (curve c), which served as catalyst for the oxidation of GSH. Meanwhile, the absorbance at 260 nm decayed with the consumption of GSH (curve b). These results were similar with the reported $Cu^{2+}$-dependent catalytic oxidization of cysteine.[38] Meanwhile, by means of electrospray ionization-mass spectrometry (ESI-MS), we also found that the amount of GSH was dramatically decreased after the addition of $Cu^{2+}$ (Fig. 3B), accompanied with the increase of GSSG level (Fig. 3C), inferring that GSH could be oxidized to GSSG by $Cu^{2+}$ catalysis in the presence of $O_2$, which was in agreement with

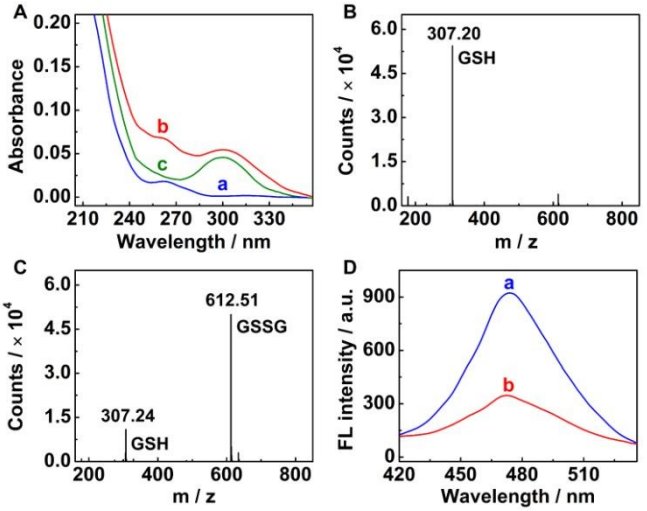


**Fig. 3** (A) UV–vis spectra of a solution of 200 μM GSH in 10 mM citrate buffer of pH 3.5, before (a) and after addition of 10 μM $Cu^{2+}$ (b: as soon as $Cu^{2+}$ is added; c: after 10 min at room temperature). ESI-MS spectra of 10 mM GSH before (B) and after (C) the addition of 200 nM $Cu^{2+}$. (D) Fluorescence signals of in situ formed CdS QDs without (a) and with (b) the catalytic oxidation of 200 nM $Cu^{2+}$ toward GSH.

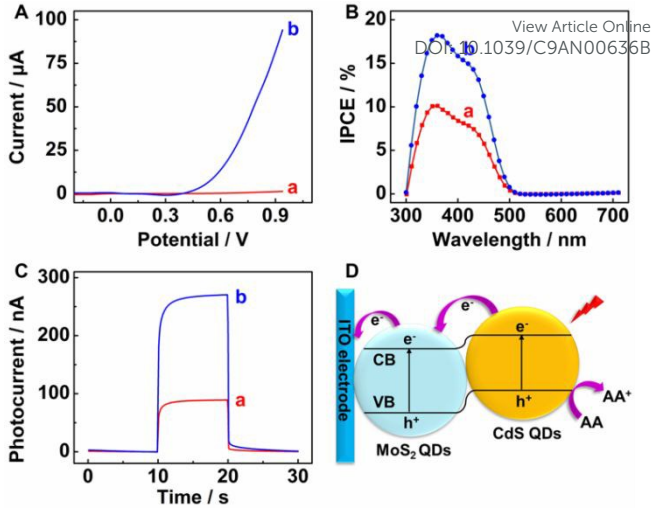


**Fig. 4** (A) I–V curves of CdS (a) and CdS/$MoS_2$ (b) modified ITO electrodes in 0.1 M PBS of pH 7.4. Scan rate: 100 mV $s^{-1}$. (B) IPCE and (C) photocurrent spectra of CdS (a) and CdS/$MoS_2$ (b) modified ITO electrodes in 0.1 M PBS of pH 7.4 containing 0.1 M AA. (D) CdS/$MoS_2$ heterojunction-based photocurrent generation mechanism.

with the previous experimental results.[18] Thus, the probable catalytic equation was described below:

$$2GSH + O_2 \xrightarrow{Cu^{2+}} GSSH + H_2O_2$$

The inhibitory action of $Cu^{2+}$ on in situ generated CdS QDs was further examined by fluorescence spectra (Fig. 3D). It can be seen that the fluorescence intensity of QDs solution was strong in the absence of $Cu^{2+}$ (curve a), and largely decreased with the lack of CdS QDs when 200 nM $Cu^{2+}$ was added as catalyst to oxidize a large number of GSH ligands (curve b). Thus, a desirable photoelectrochemical immunoassay can be constructed by means of $Cu^{2+}$-controlled in situ generation of QDs.

Electrochemical impedance spectroscopy (EIS) measurements were used for validating the preparation process of developed immunosensor after each assembly step. As shown in Fig. S2, the charge transfer resistance ($R_{ct}$) of ITO electrode was 111.7 Ω (curve a), and gradually increased to 203.8 Ω (curve b) and 305.9 Ω (curve c) when $MoS_2$ QDs and CdS QDs with poor conductivity and steric hindrance were modified, respectively. Thus, the successful preparation of immunosensor was confirmed by the increasing of $R_{ct}$.

### Characterization of CdS/$MoS_2$ heterojunction

I–V experiments were performed to investigate the formed CdS/$MoS_2$ heterostructure. As shown in Fig. 4A, the current of CdS/$MoS_2$/ITO electrode sharply increased from 0.65 V (curve b) in comparison with that of CdS/ITO electrode (curve a) due to the emerging of strong electrical breakdown.[39] Moreover, we found that incident-photon-to-current conversion efficiency (IPCE) value of CdS/$MoS_2$/ITO electrode was largely superior to that of CdS/ITO electrode (Fig. 4B), which indicated the light harvesting ability and photoelectric conversion efficiency of designed heterojunction had an enormous elevation. Thus, the significant increase of photocurrent was observed through the integration of $MoS_2$ QDs and in situ formed CdS QDs (Fig. 4C). These results suggested that the recombination of electron-hole pairs was suppressed by constructed heterostructure. The possible photocurrent generation mechanism was illustrated by Fig. 4D. Upon light irradiation, the reformed band edge in CdS/$MoS_2$ heterostructure could facilely stimulate the photoinduced electron transfer from the valence band (VB) of CdS QDs to ITO electrode, while the holes of $MoS_2$ QDs could migrate to the conduction band (CB) of CdS QDs and be sacrificed by AA, leading to the improvement of photocurrent response.

### Optimization of experimental conditions

Some experimental parameters, including $Na_2S$ concentration and incubation time of PSA with $Ab_1$, were optimized to achieve the best immunoassay for PSA. Since the added $Na_2S$ affected the amount of in situ formed CdS QDs through chemical reaction between $S^{2-}$ and $Cd^{2+}$, the photocurrent of CdS/$MoS_2$/ITO electrode was elevated with the increase of $Na_2S$ concentration up to 0.25 mM, and tended to decrease with the further addition of $Na_2S$ (Fig. S3A). Thus, 0.25 mM $Na_2S$ was used for subsequent experiments. Furthermore, the capture of PSA was essential to the subsequent assembly of CuO-$Ab_2$ probe, followed by modulating the in situ growth of CdS QDs. As shown in Fig. S3B, the photocurrent of immunosensor leveled off when the incubation time was extended to 40 min, which indicated that the immunoreaction had reached equilibrium. Thus, 40 min was selected for optimal time.

### Photoelectrochemical immunoassay

The analytical performance of developed immunosensor was evaluated under optimized conditions. Since in situ formed CdS QDs

View Article Online
DOI: 10.1039/C9AN00636B



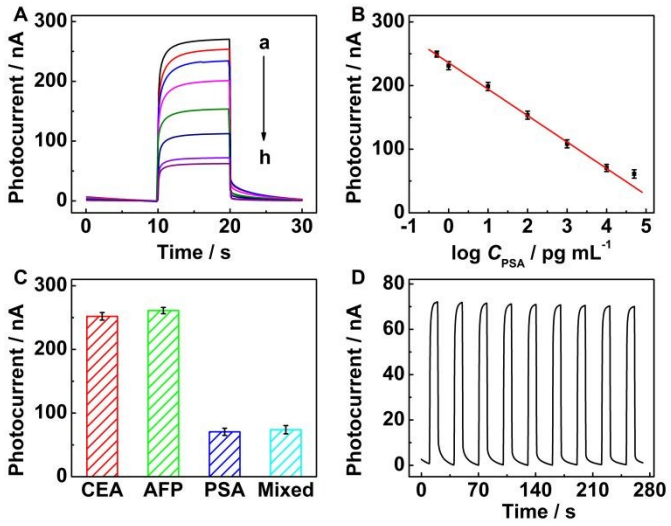


**Fig. 5** (A) Photocurrent responses of the proposed immunosensor at 0, 0.5, 1, 10, 100, 1000, 10000, 50000 pg mL$^{-1}$ target PSA (from a to h). (B) Calibration curve of photocurrent versus the logarithm of PSA concentration. (C) Specificity of photoelectrochemical immunoassay for target PSA in comparison to other interfering antigens at 10 ng mL$^{-1}$ level: CEA, AFP, and the mixed sample containing CEA, AFP and PSA. (D) Time-based photocurrent response of immunosensor.

were suppressed by $Cu^{2+}$-triggered catalytic oxidation of GSH, the photocurrent decreased as PSA level augmented (Fig. 5A). Moreover, the calibration plot showed a good linear relationship between photocurrent intensity and the logarithm of PSA concentration in the range from 0.5 pg mL$^{-1}$ to 10 ng mL$^{-1}$ (Fig. 5B). The regression equation was $I$ (nA) = 235.87 – 41.53 log $C$ (pg mL$^{-1}$) with a correlation coefficient of 0.998, where $I$ is the photocurrent detected, and $C$ is the concentration of PSA. The detection limit was estimated to be 0.29 pg mL$^{-1}$ at 3$\sigma$. Apparently, the detection performance of designed biosensor was superior or comparable to that of the previously reported immunoassays (Table S1). The high sensitivity and low detection limit was ascribed to the desirable catalytic ability of $Cu^{2+}$ and the enhancement of CdS/$MoS_2$ heterojunction. More importantly, the utilization of 96-well plate and CuO-$Ab_2$ conjugates avoided the complex interface modification procedures and expensive enzymes, respectively.

To validate the specificity of designed immunosensor, some interfering biomarkers such as CEA and AFP were chosen for the test. As depicted in Fig. 5C, the photocurrent response of target PSA was largely quenched in contrast to that of single CEA or AFP samples, and was similar to that of mixed sample containing PSA and other two interfering antigens, revealing the method had a satisfactory anti-interference ability.

The stability was also studied at 10.0 ng mL$^{-1}$ PSA. The photocurrent of prepared immunosensor still remained 97.2% of its initial value after continuous "off-on-off" light irradiation for 9 cycles (Fig. 5D). Especially, 97.5% and 94.6% of the original signal was observed when the immunosensor was stored for 1 and 2 weeks at 4 °C, respectively. The relative standard deviation (RSD) for five independent tests was 6.2%. These results substantiated an excellent stability and acceptable fabrication reproducibility for PSA assay.

### Applications in real serum samples

The feasibility of present immunosensor was verified by standard addition method. As indicated in Table S2, the test results of proposed method were 0.50 ng mL$^{-1}$ and 1.19 ng mL$^{-1}$ for the human serum samples from the First Affiliated Hospital with Nanjing Medical University, which was similar to that provided by commercial chemiluminescence immunoassay. When spiked with 2.0, 4.0, and 6.0 ng mL$^{-1}$ standard PSA solutions, the recoveries ranged from 96.5% to 105.5%. Besides, the RSD of photoelectrochemical measurements was no more than 7.12%, indicating the great potential in clinical PSA detection.

## Conclusions

In summary, we have constructed an efficient CdS/$MoS_2$ heterostructure for ultrasensitive photoelectrochemical immunoassay of PSA by using $Cu^{2+}$-triggered catalytic reaction to regulate the in situ growth of CdS QDs. The obtained heterojunction can accelerate the spatial separation of electron-hole pairs for the dramatic enhancement of photocurrent signal, and the introduction of split-type detection mode and in situ formation of QDs provide the convenient electrode assembly processes for ensuring its desirable stability and sensitivity. In the presence of PSA, $Ab_1$ can initiate the immunoreaction to capture CuO-$Ab_2$ as amplifier on 96-well plate, and its subsequent acidizing treatment releases the abundance of $Cu^{2+}$, which greatly inhibits the in situ growth of CdS QDs via the catalytic oxidization of GSH to GSSG, achieving a remarkable decrease of photocurrent in PEC system. Moreover, the developed immunosensor showed wide linear range, low detection limit and satisfactory selectivity, and successfully applied to the detection of PSA in human serum. The proposed strategy also opens up a new horizon for the design of photoelectrochenical sensing devices in biochemical analysis.

## Conflicts of interest

There are no conflicts to declare.

## Acknowledgements

We gratefully acknowledge the National Natural Science Foundation of China (Grants: 21605129, 21703199, 21675140), Postdoctoral Science Foundation of China (Grant: 2017M621830), and Jiangsu Planned Projects for Postdoctoral Research Funds (Grant: 1701187B).

## Notes and references

1 Z. Y. Cheng, N. Choi, R. Wang, S. Lee, K. C. Moon, S. Y. Yoon, L. X. Chen and J. Choo, *ACS Nano,* 2017, **11**, 4926–4933.
2 D. W. Fan, X. Ren, H. Y. Wang, D. Wu, D. Zhao, Y. C. Chen, Q. Wei and B. Du, *Biosens. Bioelectron*., 2017, **87**, 593–599.
3 B. Y. Fang, C. Y. Wang, C. Li, H. B. Wang and Y. D. Zhao, *Sens. Actuators B: Chem*., 2017, **244**, 928–933.
4 G. N. Cai, Z. Z. Yu, R. R. Ren and D. P. Tang, *ACS Sens*., 2018, **3**, 632–639.
5 L. Han, H. Q. Xia, L. Yin, V. A. Petrenko and A. H. Liu, *Biosens. Bioelectron*., 2018, **106**, 1–6.

6 K. Yang, Y. J. Hu, N. Dong, G. C. Zhu, T. F. Zhu and N. J. Jiang, *Biosens. Bioelectron*., 2017, **94**, 286–291.
7 X. Chen, W. Xu, Y. D. Jiang, G. C. Pan, D. L. Zhou, J. Y. Zhu, H. Wang, C. Chen, D. Y. Li and H. W. Song, *Nanoscale*, 2017, **9**, 16357–16364.
8 Y. X. Dong, J. T. Cao, B. Wang, S. H. Ma and Y. M. Liu, *ACS Appl. Mater. Interfaces*, 2018, **10**, 3723–3731.
9 W. J. Yao, A. Le Goff, N. Spinelli, M. Holzinger, G. W. Diao, D. Shan, E. Defrancq and S. Cosnier, *Biosens. Bioelectron.*, 2013, **42**, 556–562.
10 H. Y. Wang, C. L. Qi, W. H. He, M. H. Wang, W. J. Jiang, H. S. Yin and S. Y. Ai, *Biosens. Bioelectron.*, 2018, **99**, 281–288.
11 G. M. Wen and H. X. Ju, *Anal. Chem.*, 2016, **88**, 8339–8345.
12 L. P. Mei, F. Liu, J. B. Pan, W. W. Zhao, J. J. Xu and H. Y. Chen, *Anal. Chem.*, 2017, **89**, 6300−6304.
13 K. Y. Zhang, S. Z. Lv, Z. Z. Lin, M. J. Li and D. P. Tang, *Biosens. Bioelectron.*, 2018, **101**, 159–166.
14 J. Y. Zhuang, B. Han, W. C. Liu, J. F. Zhou, K. W. Liu, D. P. Yang and D. P. Tang, *Biosens. Bioelectron.*, 2018, **99**, 230–236.
15 M. Ehsania, M. J. Chaichi and S. N. Hosseini, *Sens. Actuators B: Chem.*, 2017, **247**, 319–328.
16 R. Grinyte, J. Barroso, B. Diez-Buitrago, L. Saa, M. Möller and V. Pavlov, *Anal. Chim. Acta*, 2017, **986**, 42–47.
17 Y. W. Wang, L. Y. Chen, M. F. Liang, H. Xu, S. R. Tang, H. H. Yang and H. B. Song, *Sens. Actuators B: Chem.*, 2017, **247**, 408–413.
18 S. R. Tang, M. L. Wang, Z. J. Li, P. Tong, Q. Chen, G. W. Li, J. H. Chen and L. Zhang, *Biosens. Bioelectron.*, 2017, **89**, 866–870.
19 J. Barroso, B. Diez-Buitrago, L. Saa, M. Möller, N. Briz and V. Pavlov, *Biosens. Bioelectron.*, 2018, **101**, 116–122.
20 T. Hou, L. F. Zhang, X. Z. Sun and F. Li, *Biosens. Bioelectron.*, 2016, **75**, 359–364.
21 X. X. Zeng, W. W. Tu, J. Li, J. C. Bao and Z. H. Dai, *ACS Appl. Mater. Interfaces*, 2014, **6**, 16197–16203.
22 D. P. Kumar, S. Hong, D. A. Reddy and T. K. Kim, *J. Mater. Chem. A*, 2016, **4**, 18551–18558.
23 S. Y. Wu, H. Huang, M. X. Shang, C. C. Du, Y. Wu and W. B. Song, *Biosens. Bioelectron.*, 2017, **92**, 646–653.
24 S. Hong, D. P. Kumar, E. H. Kim, H. Park, M. Gopannagari, D. A. Reddy and T. K. Kim, *J. Mater. Chem. A*, 2017, **5**, 20851–20859.
25 S. Iqbal, Z. W. Pan and K. B. Zhou, *Nanoscale*, 2017, **9**, 6638–6642.
26 X. L. Yin, G. Y. He, B. Sun, W. J. Jiang, D. J. Xue, A. D. Xia, L. J. Wan and J. S. Hu, *Nano Energy*, 2016, **28**, 319–329.
27 L. L. Zhao, J. Jia, Z. Y. Yang, J. Y. Yu, A. L. Wang, Y. H. Sang, W. J. Zhou and H. Liu, *Appl. Catal. B: Environ.*, 2017, **210**, 290–296.
28 D. Gopalakrishnan, D. Damien and M. M. Shaijumon, *ACS Nano*, 2014, **8**, 5297–5303.
29 P. Zhang, B. H. Xu, G. L. Chen, C. X. Gao and M. Z. Gao, *Electrochim. Acta*, 2018, **270**, 256−263.
30 M. Zhao, A. Y. Chen, D. Huang, Y. Q. Chai, Y. Zhuo and R. Yuan, *Anal. Chem.*, 2017, **89**, 8335−8342.
31 B. Mohanty, M. Ghorbani-Asl, S. Kretschmer, A. Ghosh, P. Guha, S. K. Panda, B. Jena, A. V. Krasheninnikov and B. K. Jena, *ACS Catal.*, 2018, **8**, 1683−1689.
32 H. Li, Q. Zhang, C. C. R. Yap, B. K. Tay, T. H. T. Edwin, A. Olivier and D. Baillargeat, *Adv. Funct. Mater.*, 2012, **22**, 1385–1390.
33 D. Gopalakrishnan, D. Damien, B. Li, H. Gullappalli, V. K. Pillai, P. M. Ajayan and M. M. Shaijumon, *Chem. Commun.*, 2015, **51**, 6293–6296.
34 X. J. Wang, Q. Wu, K. L. Jiang, C. X. Wang and C. Zhang, *Sens. Actuators B: Chem.*, 2017, **252**, 183–190.
35 S. Q. Zhang, X. Liu, C. B. Liu, S. L. Luo, L. L. Wang, T. Cai, Y. X. Zeng, J. L. Yuan, W. Y. Dong, Y. Pei and Y. T. Liu, *ACS Nano*, 2018, **12**, 751−758.
36 Y. Z. Liu, H. Y. Zhang, J. Ke, J. Q. Zhang, W. J. Tian, X. Y. Xu, X. G. Duan, H. Q. Sun, M. O. Tade and S. B. Wang, *Appl. Catal. B: Environ.*, 2018, **228**, 64−74.
37 W. S. Qu, Y. Y. Liu, D. B. Liu, Z. Wang and X. Y. Jiang, *Angew. Chem. Int. Ed.*, 2011, **50**, 3442–3445.
38 L. Pecci, G. Montefoschi, G. Musci and D. Cavallini, *Amino Acids*, 1997, **13**, 355–367.
39 Y. Zang, Y. Ju, X. Hu, H. Zhou, Z. J. Yang, J. J. Jiang and H. G. Xue, *Analyst*, 2018, **143**, 2895–2900.

View Article Online
DOI: 10.1039/C9AN00636B

A split-type photoelectrochemical immunoassay of PSA was developed by $Cu^{2+}$-dependent catalytic oxidation for inhibiting in situ growth of CdS QDs.